

Discovery of interlayer plasmon polaron in graphene/WS₂ heterostructures

Søren Ulstrup,^{1,*} Yann in 't Veld,² Jill A. Miwa,¹ Alfred J. H. Jones,¹ Kathleen M. McCreary,³ Jeremy T. Robinson,³ Berend T. Jonker,³ Simranjeet Singh,⁴ Roland J. Koch,⁵ Eli Rotenberg,⁵ Aaron Bostwick,⁵ Chris Jozwiak,⁵ Malte Rösner,^{2,†} and Jyoti Katoch^{4,‡}

¹*Department of Physics and Astronomy,
Interdisciplinary Nanoscience Center,
Aarhus University, 8000 Aarhus C, Denmark*

²*Institute for Molecules and Materials,
Radboud University, 6525 AJ Nijmegen, the Netherlands*

³*Naval Research laboratory, Washington, D.C. 20375, USA*

⁴*Department of Physics, Carnegie Mellon University,
Pittsburgh, Pennsylvania 15213, USA*

⁵*Advanced Light Source, E. O. Lawrence Berkeley
National Laboratory, Berkeley, California 94720, USA*

Harnessing electronic excitations involving coherent coupling to bosonic modes is essential for the design and control of emergent phenomena in quantum materials [1]. In situations where charge carriers induce a lattice distortion due to the electron-phonon interaction, the conducting states get “dressed”. This leads to the formation of polaronic quasiparticles that dramatically impact charge transport, surface reactivity, thermoelectric and optical properties, as observed in a variety of crystals and interfaces composed of polar materials [2–6]. Similarly, when oscillations of the charge density couple to conduction electrons the more elusive plasmon polaron emerges [7], which has been detected in electron-doped semiconductors [8–10]. However, the exploration of polaronic effects on low energy excitations is still in its infancy in two-dimensional (2D) materials. Here, we present the discovery of an interlayer plasmon polaron in heterostructures composed of graphene on top of SL WS₂. By using micro-focused angle-resolved photoemission spectroscopy (microARPES) during *in situ* doping of the top graphene layer, we observe a strong quasiparticle peak accompanied by several carrier density-dependent shake-off replicas around the SL WS₂ conduction band minimum (CBM). Our results are explained by an effective many-body model in terms of a coupling between SL WS₂ conduction electrons and graphene plasmon modes. It is important to take into account the presence of such interlayer collective modes, as they have profound consequences for the electronic and optical properties of heterostructures that are routinely explored in many device architectures involving 2D transition metal dichalcogenides (TMDs) [11–15].

Sophisticated heterostructure designs involving 2D crystals with pre-defined lattice mismatch and interlayer twist angle have emerged as promising platforms for tailoring potential energy surfaces and excitations in solid state quantum simulators [14, 15]. While these systems leverage fine-control of complex lattice structures and quantum states, the close proximity of materials may further induce additional interlayer correlation effects [16]. For example, in heterostructures composed of graphene and semiconducting TMDs, superlattice bands are generated concomitant with screening-induced band shifts that dictate quasiparticle band alignments and gaps [17–20]. Intriguingly, recent experiments on twisted bilayer graphene interfaced with SL WSe₂ point towards even richer interactions, as the presence

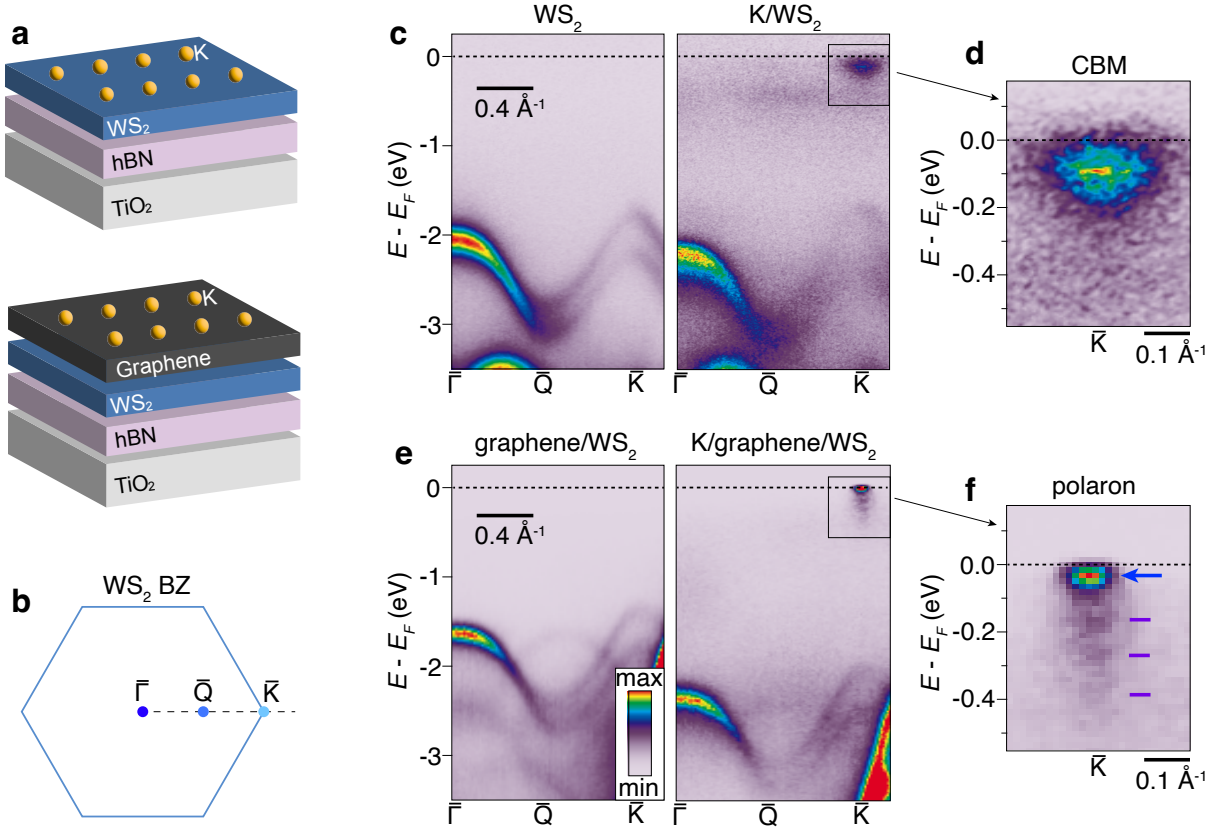


FIG. 1. Quasiparticle bands of electron-doped WS_2 heterostructures. **a**, Layout of systems with doping achieved by deposition of potassium atoms. **b**, Brillouin zone (BZ) of SL WS_2 with ARPES measurement direction marked by a dashed line. **c**, ARPES spectra of bare (left panel) and potassium doped WS_2 (right panel) supported on hBN. The achieved electron density in the strongly doped case is estimated to be $3.0 \cdot 10^{13} \text{ cm}^{-2}$. **d**, Close-up of the CBM region marked in (c). **e-f**, Corresponding ARPES spectra for WS_2 with graphene on top. The achieved electron density in the potassium-doped graphene layer is $4.8 \cdot 10^{13} \text{ cm}^{-2}$. The close-up of the CBM region of WS_2 in (f) reveals the formation of a polaron via a sharp quasiparticle peak, which is demarcated by a blue arrow, and several shake-off replicas marked by purple ticks.

of SL WSe_2 stabilises superconductivity below the magic twist angle of bilayer graphene [13]. In SL WS_2 contacted with the topological insulator Bi_2Se_3 , interlayer exciton-phonon bound states have been detected [21]. Such observations point to the importance of interlayer collective excitations involving bosonic modes.

We endeavour to determine how the electronic excitation spectrum of a representative semiconducting SL TMD is affected by a doped graphene overlayer, as is present in a variety of device architectures [22–27]. To this end, we focus on SL WS_2 as this material exhibits a direct band gap at the $\bar{\text{K}}$ -point of the Brillouin zone (BZ) and a large spin-orbit coupling

(SOC) induced splitting of the valence bands, allowing to simultaneously resolve energy- and momentum-dependent electronic excitations around the valence and conduction band extrema using high-resolution ARPES [28, 29]. The heterostructures are supported on 10-30 nm thick hBN, which serves two purposes: (i) it replicates the heterostructures that are typically used in transport and optical measurements, and (ii) provides an atomically flat and inert interface that preserves the salient dispersion of SL WS₂, since hybridization is strongly suppressed due to the large band gap of hBN [28]. The entire stack is placed on degenerately-doped TiO₂ in order to prevent charging during photoemission. The quasiparticle band structure from the heterostructure is spatially-resolved using microARPES during *in situ* electron doping by depositing potassium atoms on the surface. In order to determine the effect of the graphene overlayer, we measure two types of heterostructures - one with graphene and one without. A schematic of our doped heterostructures is presented in Fig. 1(a). Spectra are collected along the $\bar{\Gamma}$ - \bar{Q} - \bar{K} direction of the SL WS₂ BZ, as sketched in Fig. 1(b).

Figure 1(c) presents ARPES spectra of the effect of strong electron-doping on bare WS₂ with potassium atoms deposited directly on the surface. Before doping, the expected band structure of SL WS₂ is observed with a local valence band maximum (VBM) at $\bar{\Gamma}$ and a global VBM at \bar{K} , a total gap larger than 2 eV and a SOC splitting of 430 meV in the VBM [30] (see left panel of Fig. 1(c)). At an estimated highest electron density of $3.0 \cdot 10^{13}$ cm⁻², induced by the adsorbed potassium atoms, the CBM is populated and the shape of the VBM is strongly renormalized, as observed in the right panel of Fig. 1(c) and previously reported [28]. The direct band gap at \bar{K} is furthermore reduced to (1.64 ± 0.02) eV (Extended data Fig. 1), indicating enhanced internal screening. A detailed view of the CBM region in Fig. 1(d), reveals the CBM to be relatively broad with an energy distribution curve (EDC) linewidth of (0.17 ± 0.02) eV and a momentum distribution curve (MDC) width of (0.29 ± 0.02) Å⁻¹ (Extended data Fig. 2).

These spectra are contrasted with the situation where a graphene layer is placed on top of WS₂ in Fig. 1(e). In the undoped case shown in the left panel of Fig. 1(e), the bands exhibit the same general features as seen in the left panel of Fig. 1(c), although they are noticeably sharper and shifted towards the Fermi energy due to the additional screening of the Coulomb interaction by the graphene [18]. Furthermore, a replica of the WS₂ local VBM around $\bar{\Gamma}$ is noticeable close to \bar{Q} due to the superlattice formed between graphene

and WS₂ [19]. Upon doping graphene to an electron density of about $4.8 \cdot 10^{13} \text{ cm}^{-2}$, the SL WS₂ valence band shifts down in energy and the shape of the VBM does not renormalize as in the case of bare WS₂ (see right panel of Fig. 1(e)). The total gap is now $(2.04 \pm 0.02) \text{ eV}$ (Extended data Fig. 1), indicating that the non-local Coulomb interaction in WS₂ is not fully suppressed. However, the CBM region looks dramatically different, as seen by comparing Figs. 1(f) and 1(d). In the situation with a doped graphene overlayer, a sharp quasiparticle peak occurs. The peak is accompanied by a series of replica bands towards lower kinetic energy, that are conventionally called shake-off bands. The EDC and MDC linewidths of the main quasiparticle peak are reduced by around a factor of 4, compared to bare K/WS₂ (Extended data Fig. 2). The feature bears resemblance to a Fröhlich polaron that is observable in ARPES when the conducting electrons couple strongly to phonons [2, 3, 6, 31].

Density functional theory (DFT) calculations for the K/graphene/WS₂ heterostructure (see Methods and Extended data Figs. 3-4) confirm the experimental results which show that the graphene Dirac bands do not strongly hybridize with the WS₂ CBM at \bar{K} . As a result, there is only a vanishingly small charge transfer from the strongly K doped graphene layer to the WS₂ layer. This explains the experimental observation of strongly doped graphene, accompanied by the small \bar{K} valley occupation in WS₂. This also explains the absence of VBM renormalization in WS₂ covered by graphene, as this only occurs at carrier concentrations larger than $2.0 \cdot 10^{13} \text{ cm}^{-2}$ in WS₂ [28]. These DFT calculations, however, do not reproduce the still significant band gap or the shake-off bands, pointing towards the important role played here by many-body interactions, that are beyond the scope of DFT calculations.

In order to understand the origin of the shake-off bands in the dispersion at \bar{K} in the graphene/WS₂ heterostructure, we tune the charge carrier density by sequentially increasing the amount of adsorbed potassium on graphene. After each dosing step we measure both the WS₂ conduction band region and the graphene Dirac cone to correlate the evolution of the shake-off bands spectral line shapes with the filling of the Dirac cone. Second derivative plots of the ARPES intensity are shown in Fig. 2(a) to highlight the relatively faint shake-off bands compared to the intense quasiparticle peak for a range of doping where the graphene carrier concentration is varied over a range of $1.0 \cdot 10^{13} \text{ cm}^{-2}$. Corresponding EDCs with fits to Lorentzian components are shown in Fig. 2(b). The extraction of the graphene wave vector k_F from measurements of the Dirac cone Fermi surface is illustrated in Fig.

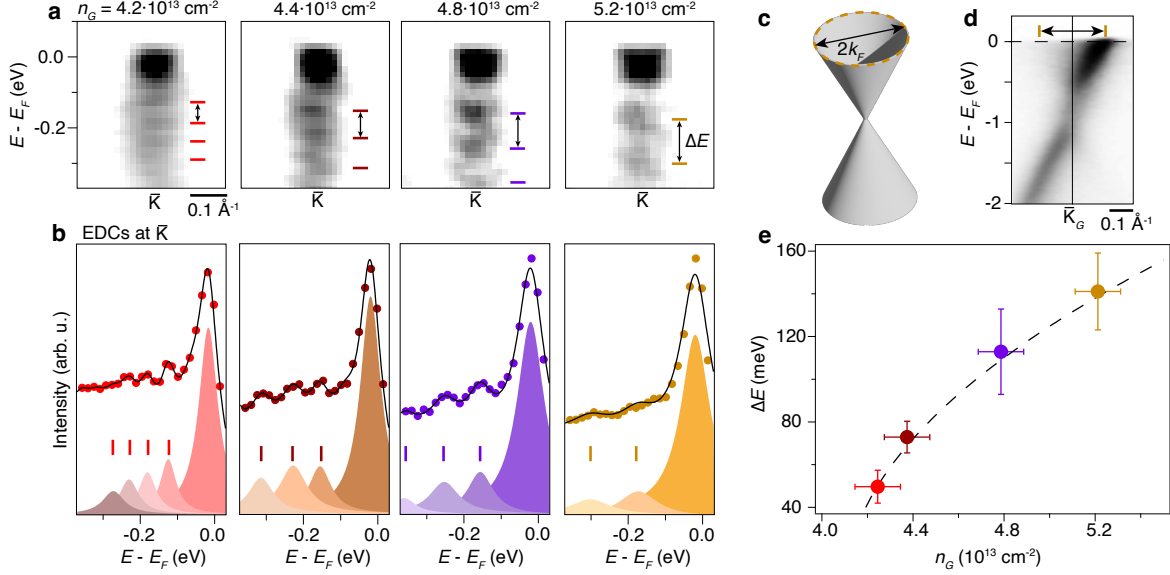


FIG. 2. Doping-dependence of shake-off bands. **a**, Second-derivative ARPES intensity in the CBM region of potassium doped graphene/WS₂ at the given electron density in graphene (n_G). Ticks demarcate shake-off bands and the double-headed arrows indicate their energy separation (ΔE). **b**, Energy distribution curves (EDCs) with fits (black curves) to Lorentzian components on a linear background. Peak components are shown with fitted positions marked by colored ticks. **c**, Sketch of graphene Dirac cone and Fermi surface (dashed circle) measured simultaneously by ARPES at each doping step. **d**, ARPES spectrum of potassium doped graphene on WS₂ with diameter of Fermi surface ($2k_F$) indicated by double-headed arrow. The spectrum is for the maximum achieved doping of graphene of $5.2 \cdot 10^{13} \text{ cm}^{-2}$. **e**, Increase of shake-off energy separation with graphene doping extracted from the analysis. The dashed line is a fit to a function proportional to $\sqrt{n_G}$.

2(c) and demonstrated by a measurement of doped graphene on WS₂ in Fig. 2(d). The EDC analysis of the shake-off bands as a function of graphene doping reveals the energy separation between shake-off bands increases from $(50 \pm 8) \text{ meV}$ to $(141 \pm 18) \text{ meV}$ and that the increase is proportional to $\sqrt{n_G}$, as shown in Fig. 2(e). Furthermore, the EDC fits in Fig. 2(b) demonstrate that the shake-off band intensity relative to the main quasiparticle peak diminishes with doping.

These observations provide further clues on the origin of the shake-off bands. An internal coupling between WS₂ conducting electrons and phonons can be ruled out, because the energy separation of the shake-off bands at high doping exceeds the WS₂ phonon bandwidth of 55 meV [32]. Given the significant doping of graphene, there are, however, two other bosonic excitations that could be responsible for the shake-off bands in WS₂: phonons and plasmons in graphene. In doped graphene there are indeed phonons with energies between

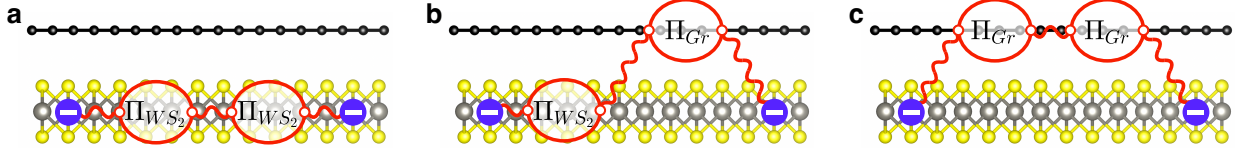


FIG. 3. Illustrations of the Coulomb interaction in WS_2 and its screening channels in graphene/ WS_2 heterostructures. Wavy lines and “bubbles” represent bare Coulomb interactions and polarization processes, respectively. **a**, Coulomb interaction and screening from WS_2 only. **b**, Illustration of mixed screening channels from WS_2 and graphene. **c**, Coulomb interaction between electrons in WS_2 screened by graphene polarization processes only, which couple graphene plasmons to the WS_2 Coulomb interaction. Interlayer polarization effects are suppressed due to the vanishingly small hybridization between the WS_2 $\bar{\text{K}}$ valley and graphene’s Dirac cone.

150 and 200 meV with significant electron-phonon coupling. These phonon energies change, however, only by up to 20 meV upon tuning the electron doping [33, 34] and can thus be ruled out as the origin for the observed shake-offs. In stark contrast, plasmons in 2D materials are known to be significantly affected by the doping level of the system. Indeed, significant plasmon excitations have been observed in graphene in the regime of doping we are considering [35]. Moreover, the doping dependence of the line shape of the shake-off bands is consistent with graphene plasmon excitations coupling to the WS_2 conduction electrons [7–10]. Taken together, this suggests that the observed feature is an interlayer plasmon polaron with unusually sharp line shapes and well-defined shake-offs, unlike the previously observed plasmonic polarons in electron-doped bulk materials [8, 9] and in internally doped SL MoS_2 [10].

To theoretically substantiate this interpretation, we use a generic model consisting of two layers, one with a parabolic electronic spectrum mimicking the occupied WS_2 $\bar{\text{K}}$ -valley and one with the conventional Dirac spectrum of graphene. As justified by our DFT calculations, we assume that the two layers are electronically decoupled, such that the only coupling between them is the long-range Coulomb interaction. Based on this model, we perform random phase approximation (RPA) calculations to evaluate the momentum-dependent and dynamically screened density-density Coulomb interaction matrix $\mathbf{W}_q(\omega)$ in the WS_2 /graphene layer basis. In Fig. 3 we depict the possible screening channels to the Coulomb interaction between electrons within the WS_2 layer, which can be categorized into WS_2 screening only [Fig. 3(a)], mixed screening from WS_2 and graphene [Fig. 3(b)], and pure graphene screening [Fig. 3(c)]. We subsequently use $\mathbf{W}_q(\omega)$ within a G_0W_0 framework to calculate

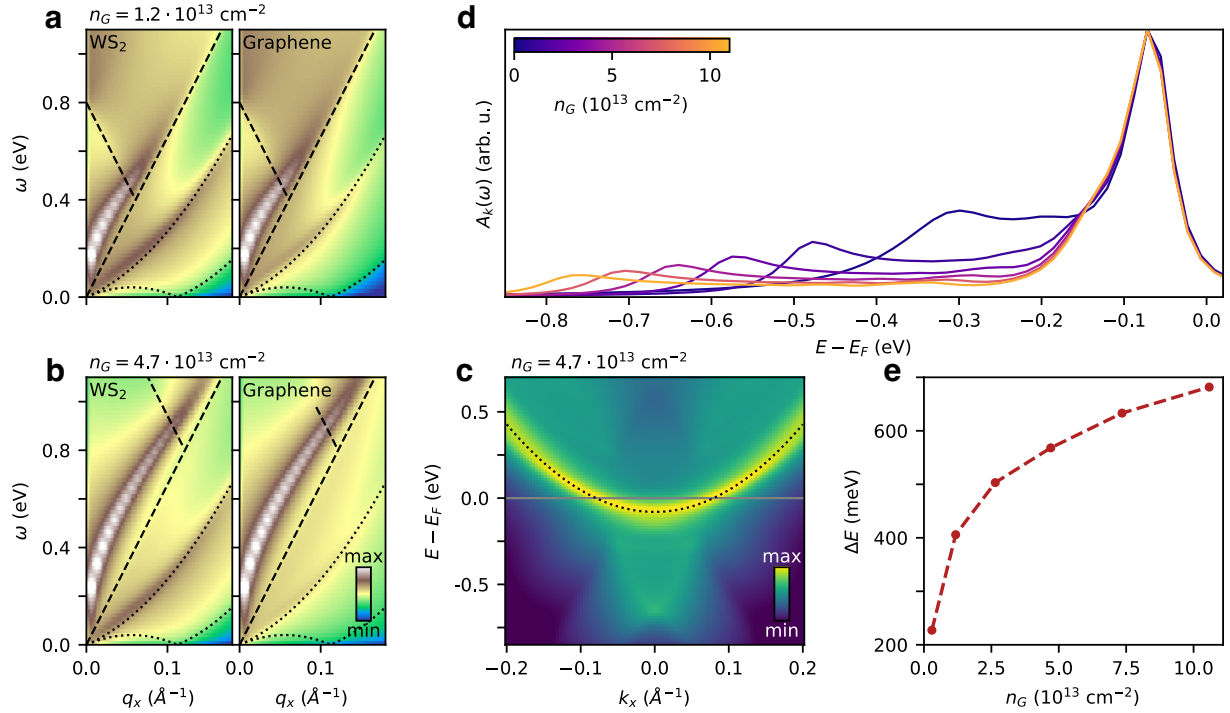


FIG. 4. Theoretical G_0W_0 results. **a-b**, Spectral function $B_q(\omega)$ of the Coulomb interaction in the WS_2 (left) and graphene (right) channels, for two different graphene occupations n_G . Dotted and dashed lines indicate the edges of the electron-hole continua of WS_2 and graphene, respectively. **c**, Momentum resolved WS_2 normal state spectral function $A_k(\omega)$. The dotted black line represents the bare WS_2 dispersion. **d**, EDCs of the WS_2 normal state spectral function at \bar{K} for a variety of graphene occupations. **e**, Energy splitting ΔE between the WS_2 quasiparticle peak and the plasmon polaron peak as a function of graphene occupation.

the interacting spectral function within the effective WS_2 \bar{K} -valley.

In Figs. 4(a) and 4(b) we show elements of $\mathbf{B}_q(\omega) = -\pi^{-1}\text{Im}[\mathbf{W}_q(\omega)]$, which is proportional to the momentum resolved electron energy loss spectrum $\text{EELS}_q(\omega)$, within the WS_2 (left panels) and graphene (right panels) layers for two different graphene carrier concentrations. Within the graphene layer, we find a strong plasmonic resonance with the characteristic \sqrt{q} -like dispersion [36, 37], which is damped as soon as it enters graphene's particle-hole continuum indicated by black dashed lines. Upon doping graphene, the plasmon dispersion shifts to higher energies, but maintains its \sqrt{q} -like dispersion. Within the WS_2 layer, we find two distinct branches, corresponding to two different plasmonic modes. The lower branch closely follows the original WS_2 plasmon dispersion which we would find upon excluding interlayer Coulomb coupling from processes as those illustrated in Figs. 3(b)-(c),

such that we identify this branch as a WS₂ intralayer plasmon dominated one. The upper branch arises from the interlayer Coulomb coupling and closely follows the graphene plasmon dispersion. The graphene plasmon dispersion thus strongly couples into the screened Coulomb interaction within the WS₂ layer. This is a consequence of the vastly different electron densities in the two layers and the enhanced graphene Landau damping region, which overlaps the undamped (q, ω) area of the WS₂ polarization. This finally leads to a strong suppression of the WS₂ plasmonic features within both layers and is a result of the significantly larger Fermi velocity in graphene. As a consequence, the dynamics of the WS₂ Coulomb interaction is dominated by screening from the graphene layer as illustrated in Fig. 3(c), and is therefore highly dependent on the graphene doping through its plasmon.

In Fig. 4(c) we show the resulting dressed spectral function $A_k(\omega) = -\pi^{-1}\text{Im}[G_k(\omega)]$ within the effective WS₂ \bar{K} -valley for a graphene doping of $n_G = 4.7 \cdot 10^{13} \text{ cm}^{-2}$. In qualitative agreement with the ARPES spectrum, we find a pronounced plasmon polaron band below the original CBM separated by an energy ΔE . In Fig. 4(d) we further show EDCs of the spectral function $A_k(\omega)$ at the center of the conduction band for a variety of graphene occupations. In all of these linecuts we can identify the main quasiparticle around $E - E_F \approx -0.08 \text{ eV}$, and the plasmon polaron bands at lower energies. As the graphene occupation increases, the plasmon polaron band shifts to lower energies, increases its separation from the main quasiparticle peak, and loses intensity. The energy splitting ΔE is plotted as a function of graphene doping n_G in Fig. 4(e), where we find the same $\sqrt{n_G}$ -like behaviour as observed in our ARPES measurement. This trend is fully driven by the graphene plasmon and is unaffected by the WS₂ polarization as discussed in the Extended Material.

The higher order shake-off bands are missing as a result of the G_0W_0 approximation and can only be described by taking vertex corrections into account [10, 38, 39]. Missing vertex corrections [38–40] and underestimated external (substrate) screening (see Extended Material) are reasons for the theoretically estimated ΔE being larger than the experimental ones. To obtain a quantitative agreement, we would additionally need to derive all model parameters from first principle calculations based on the full non-commensurate supercell heterostructures and taking SOC effects into account. However, the details of the parameters do not influence the qualitative behaviour of the theoretical results as shown in Extended data Fig. 5. The qualitative agreement between our theoretical and experimental results is thus striking, such that we conclude that the observed shake-off bands in WS₂ are induced

by the graphene plasmon, forming interlayer plasmonic polaron satellites in WS_2 .

The impact of this finding could be far-reaching, as interfaces between graphene and TMDs have been exploited in various ways: to induce large spin-orbital proximity effects [12], for the stabilization of superconductivity below magic angle twists in bilayer graphene interfaced with WSe_2 [13], or for charge carrier control of Wigner crystallization and realizations of discrete Mott states in dual-gated TMD heterobilayers contacted with graphite [14, 15]. Our observation of interlayer polaronic quasiparticles induced by adding charge to a contacting graphene layer will thus be important to consider in the interpretation and modelling of device measurements. Further experiments will be required to evaluate their impact on the optoelectronic properties and band engineering of heterostructures as well as their utility for ultrathin photonics and plasmonic devices.

ACKNOWLEDGEMENT

Y.I.V. and M.R. thank G. Ganzevoort for useful discussions. J.K. acknowledges funding from the U.S. Department Office of Science, Office of Basic Sciences, of the U.S. Department of Energy under Award No. DE-SC0020323 as well as partial support by the Center for Emergent Materials, an NSF MRSEC, under award number DMR-2011876. S.U. acknowledges funding from the Danish Council for Independent Research, Natural Sciences under the Sapere Aude program (Grant No. DFF-9064-00057B) and from the Novo Nordisk Foundation (Grant NNF22OC0079960). J.A.M acknowledges funding from the Danish Council for Independent Research, Natural Sciences under the Sapere Aude program (Grant No. DFF-6108-00409) and the Aarhus University Research Foundation. S.S. acknowledges the support from National Science Foundation under grant DMR-2210510 and the Center for Emergent Materials, an NSF MRSEC, under award number DMR-2011876. K.M.M, J.T.R. and B.T.J. acknowledge support from core programs at the Naval Research Laboratory. Y.I.V and M.R. acknowledge support from the Dutch Research Council (NWO) via the “TOPCORE” consortium. M.R. acknowledges partial support by the European Commission’s Horizon 2020 RISE program Hydrotronics (Grant No. 873028).

AUTHOR INFORMATION

Correspondence and requests for materials should be addressed to:

S.U. (ulstrup@phys.au.dk).

M.R. (m.roesner@science.ru.nl).

J. K. (jkatoch@andrew.cmu.edu).

SUPPORTING INFORMATION

Fabrication of heterostructures

First, bulk hBN crystals (commercial crystal from HQ Graphene) were exfoliated onto 0.5 wt% Nb-doped rutile $\text{TiO}_2(100)$ substrate (Shinkosha Co., Ltd) using scotch tape to obtain 10-30 nm thick hBN flakes. Next, we transferred chemical vapor deposition (CVD) grown SL WS_2 onto a selected thin hBN flake using a thin polycarbonate film on a polydimethylsiloxane stamp using a custom-built transfer tool. This was followed by transfer of CVD graphene on top of the WS_2/hBN stack. The details of the CVD growth of SL WS_2 and graphene as well as transfer process were previously provided in Ref. 19. After each transfer process, the sample surface was cleaned by annealing in ultrahigh vacuum (UHV) at 150 °C for 15 mins to remove any unwanted residues or adsorbates from the surface.

Micro-focused angle-resolved photoemission spectroscopy

The photoemission experiments were carried out in the microARPES end-station of the MAESTRO facility at the Advanced Light Source. Samples were transported through air and given a 1 hour anneal at 500 K in the end-station prior to measurements. The base pressure of the system was better than $5 \cdot 10^{-11}$ mbar and the samples were kept at a temperature of 78 K throughout the measurements.

Energy- and momentum-resolved photoemission spectra were measured using a Scienta R4000 hemispherical electron analyser with custom-made deflectors. All samples were aligned with the $\bar{\Gamma} - \bar{K}$ direction of the WS_2 Brillouin zone (BZ) aligned along the slit of the analyser. Measurements on WS_2 samples without a graphene overlayer were performed with a photon energy of 145 eV, while measurements on samples with a graphene

overlayer were done with a photon energy of 80 eV. These energies were chosen on the basis of photon energy scans revealing the optimum matrix elements for clearly resolving the WS₂ and graphene band structures. The photon beam was focused to a spot-size with a lateral diameter of approximately 10 μm using Kirkpatrick-Baez (KB) mirrors.

Electron-doping of samples was achieved by depositing potassium (K) from a SAES getter source *in situ*. Each dose had a duration of 40 s. After each dose, the $\bar{\Gamma} - \bar{K}$ cut of WS₂ was acquired for 5 minutes followed by a measurement around the Dirac point of graphene for 3 minutes. Efficient switching between these two cut directions was achieved using the deflector capability of the analyser, such that all measurements could be done with the sample position held fixed. In WS₂ without a graphene overlayer, the carrier concentration in WS₂ was estimated using the Luttinger theorem via the Fermi surface area enclosed by the WS₂ conduction band. In the samples with a graphene overlayer, we determined the doping of graphene by directly measuring k_F , as shown in Figs. 2(c) and 2(d) in the main paper, and use the relation $n_G = k_F^2/\pi$.

The second derivative plots of the ARPES intensity shown in Fig. 2(a) of the main paper were obtained using the method described in Ref. 41 and merely used as a tool to visualize the data. Analysis of energy and momentum distribution curves were always performed on the raw ARPES intensity.

A total of 3 samples were studied, which were a bare WS₂ and two graphene/WS₂ heterostructures on separate TiO₂ wafers such that fresh doping experiments could be performed on all samples. The two graphene/WS₂ heterostructures exhibited twist angles of $(7.5 \pm 0.3)^\circ$ and $(18.1 \pm 0.3)^\circ$ between graphene and WS₂, as determined from the BZ orientations in the ARPES measurements. We found identical behaviors with doping and formation of polarons in the two heterostructures, confirming the reproducibility of our results.

Density Functional Theory Calculations

To study the hybridization and the possible charge transfer between the graphene and WS₂ layers, we performed density functional theory (DFT) calculations using a 4×4 WS₂ / 5×5 graphene supercell with K doping, as indicated in Fig. 7. The supercell height has been fixed to about 26 Å to suppress unwanted wavefunction overlap between adjacent supercells. The WS₂ lattice constant has been fixed to its experimental value of 3.184 Å

while the graphene lattice constant has been strained by about 3% to 2.547 Å to obtain a commensurable heterostructure. The graphene-WS₂ interlayer separation has been set to previously reported 3.44 Å [42] and the K-graphene distance has been optimized in DFT yielding 2.642 Å in the out-of-plane direction. All calculations were performed within the Vienna Ab initio Simulation Package (VASP) [43, 44] utilizing the projector-augmented wave (PAW) [45, 46] formalism within the PBE [47] generalized-gradient approximation (GGA) using $12 \times 12 \times 1$ k point grids and an energy cut-off of 400 eV.

In Fig. 8 we show the resulting unfolded band structure (without SOC effects) together with the pristine WS₂ band structure (including SOC effects) following the approach from Ref. [48] as implemented in [49]. From this we can clearly see that in the heterostructure new states in the gap of WS₂ arise, which we identify as graphene bands. Due to unfolding (matrix element) effects, the second linear band forming graphene’s Dirac cone is not visible. Upon unfolding to the primitive graphene structure, the Dirac point becomes visible (right panel) showing a graphene Fermi energy of about 0.6 eV in good agreement with the experimentally achieved range. In the upmost valence states around the \bar{K} -point, we see that the graphene and WS₂ bands hybridize similar to reported band structures on undoped graphene/WS₂ [42, 50]. In the conduction band region, we however see that graphene states are far from the \bar{K} -valley, such that hybridization between graphene p_z and W d_{z^2} orbitals (which are dominating the \bar{K} -valley) is almost completely suppressed. As a result, there is negligible charge transfer from graphene to WS₂, so that primarily graphene is doped by potassium. This is fully in line with our experimental results.

G₀W₀ calculations

We can consider the WS₂ layer to be weakly doped and the \bar{K} -valley to be electronically decoupled from the strongly doped graphene layer. Consequently, we can approximate the WS₂ \bar{K} -valley dispersion by a single-band effective mass model $\xi_k = k^2/(2m^*) - \mu_{\text{WS}_2}$, with μ_{WS_2} the WS₂ chemical potential and neglecting SOC effects. Due to the electronic decoupling, the two layers only interact via the long-range Coulomb interaction.

The WS₂ effective-mass was set to $m^* = 0.3m_e$. The interlayer distance, WS₂ and graphene unit-cell areas and internal dielectric constants were fixed to $d = 3 \text{ \AA}$, $A_{\text{WS}_2} = 8.79 \text{ \AA}^2$, $A_{\text{Gr}} = 5.27 \text{ \AA}^2$, $\epsilon_{\text{WS}_2} = 8.57$ and $\epsilon_{\text{Gr}} = 2.0$, respectively. Additionally, the external

dielectric constant was set to $\varepsilon_{ext} = 3$, close to the value of hBN, and the material heights were set to $h_{\text{WS}_2} = 6.16 \text{ \AA}$ and $h_{\text{Gr}} = 3.35 \text{ \AA}$ for WS_2 and graphene, respectively, in accordance with Refs. [51, 52]. We set the WS_2 chemical potential to $\mu_{\text{WS}_2} = 0.04 \text{ eV}$ such that WS_2 had an occupation of $n = 1.7 \cdot 10^{13} \text{ cm}^{-2}$ and varied the graphene chemical potential to simulate various graphene occupations. The G_0W_0 calculations were performed with the TRIQS [53] and TPRF [54] packages, using 300×300 momentum meshes and 500 linearly spaced frequency points from -4.0 eV to 4.1 eV , with a broadening of $\delta = 0.02 \text{ eV}$.

In order to describe the non-local and dynamic screening of the heterostructure, we calculated the screened Coulomb matrix $\mathbf{W}_q(\omega)$ in the random phase approximation (RPA), neglecting non-density-density terms. Due to the negligible interlayer hybridization, the density-density RPA polarization $\mathbf{\Pi}_q(\omega)$ is approximately block diagonal,

$$\mathbf{\Pi}_q(\omega) = \begin{bmatrix} \Pi_q^{\text{WS}_2}(\omega) & 0 \\ 0 & \Pi_q^{\text{Gr}}(\omega) \end{bmatrix}, \quad (1)$$

such that for both the WS_2 block $\Pi_q^{\text{WS}_2}(\omega)$ and the graphene block $\Pi_q^{\text{Gr}}(\omega)$ we can independently use analytic zero-temperature expressions for a quadratic [55] and a Dirac dispersion [56, 57], respectively.

The bare density-density Coulomb matrix elements were approximated by

$$\mathbf{V}_q = V_q \begin{bmatrix} 1 & e^{-qd} \\ e^{-qd} & 1 \end{bmatrix}, \quad (2)$$

where d is the interlayer distance and V_q is given by $V_q = 2\pi e^2 / (A\varepsilon_q q)$, with $A = (A_{\text{WS}_2} + A_{\text{Gr}})/2$ the layer-averaged unit cell area and e the electron charge. ε_q is a dielectric function capturing the neglected non-metallic screening channels and is given by [58]

$$\varepsilon(q) = \varepsilon_{int} \frac{1 - \tilde{\varepsilon}^2 e^{-2qh}}{1 + 2\tilde{\varepsilon} e^{-qh} + \tilde{\varepsilon}^2 e^{-2qh}}, \quad (3)$$

with $\tilde{\varepsilon} = (\varepsilon_{int} - \varepsilon_{ext}) / (\varepsilon_{int} + \varepsilon_{ext})$ and $h = h_{\text{WS}_2} + h_{\text{Gr}}$ the total thickness of the heterostructure. The internal dielectric constant is set to the average value of WS_2 and graphene, i.e., $\varepsilon_{int} = (\varepsilon_{\text{WS}_2} + \varepsilon_{\text{Gr}})/2$. The screened density-density Coulomb interaction is finally given as

the matrix product $\mathbf{W}_q(\omega) = (\mathbf{I} - \mathbf{V}_q \mathbf{\Pi}_q(\omega))^{-1} \mathbf{V}_q$, with \mathbf{I} the identity matrix.

To explain the experimental observation of plasmon polaron bands in the doped graphene/WS₂ heterostructure we need to theoretically describe the effect of the non-local and dynamic Coulomb interaction on the WS₂ normal state, for which we performed G₀W₀ calculations. The negligible hybridization between the layers renders both the bare electron propagator $\mathbf{G}^{(0)}$ and the G₀W₀ self-energy $\mathbf{\Sigma}$ approximately block diagonal. As a consequence, one only requires information about the screened Coulomb interaction within the WS₂ layer, $W_q^{\text{WS}_2}(\omega)$, to determine the renormalization of the WS₂ normal state. The self-energy is therefore given by

$$\Sigma_k^{\text{WS}_2}(i\omega_n) = -\frac{1}{\beta} \sum_{q,m} G_{k+q}^{(0),\text{WS}_2}(i\omega_n + i\omega_m) W_q^{\text{WS}_2}(i\omega_m), \quad (4)$$

where $G_k^{(0),\text{WS}_2}(i\omega_n) = 1/(i\omega_n - \xi_k)$. In spectral representation the sum over discrete Matsubara frequencies can be performed analytically, such that on the real-frequency axis

$$\Sigma_k^{\text{WS}_2}(\omega) = -\sum_q V_q n_F(\xi_{k+q}) + \sum_q \int d\omega' B_q(\omega') \frac{n_B(\omega') + n_F(\xi_{k+q})}{\omega + i\delta + \omega' - \xi_{k+q}}, \quad (5)$$

where $B_q(\omega) = -\pi^{-1} \text{Im}(W_q^{\text{WS}_2}(\omega) - V_q)$ and n_F and n_B are the Fermi-Dirac and Bose-Einstein distribution functions, respectively. To compare to ARPES measurements we calculated the WS₂ spectral-function as $A_k^{\text{WS}_2}(\omega) = -\pi^{-1} \text{Im}(G_k^{\text{WS}_2}(\omega))$, where $G_k^{\text{WS}_2}(\omega) = 1/(\omega + i\delta - \xi_k - \Sigma_k^{\text{WS}_2}(\omega))$.

In Fig. 9 we show the spectral function of WS₂ and the resulting ΔE (as insets) for various further model parameters. From these additional calculations, we understand that the WS₂ polarization does not play a significant role for the interlayer plasmon polaron formation and that the effective distance, effective mass, and effective external screening only quantitatively affect the shake-off band splitting. Note that increasing the effective external screening (as resulting from the substrate) from $\varepsilon_{ext} = 3$ to $\varepsilon_{ext} = 6$ reduces ΔE significantly.

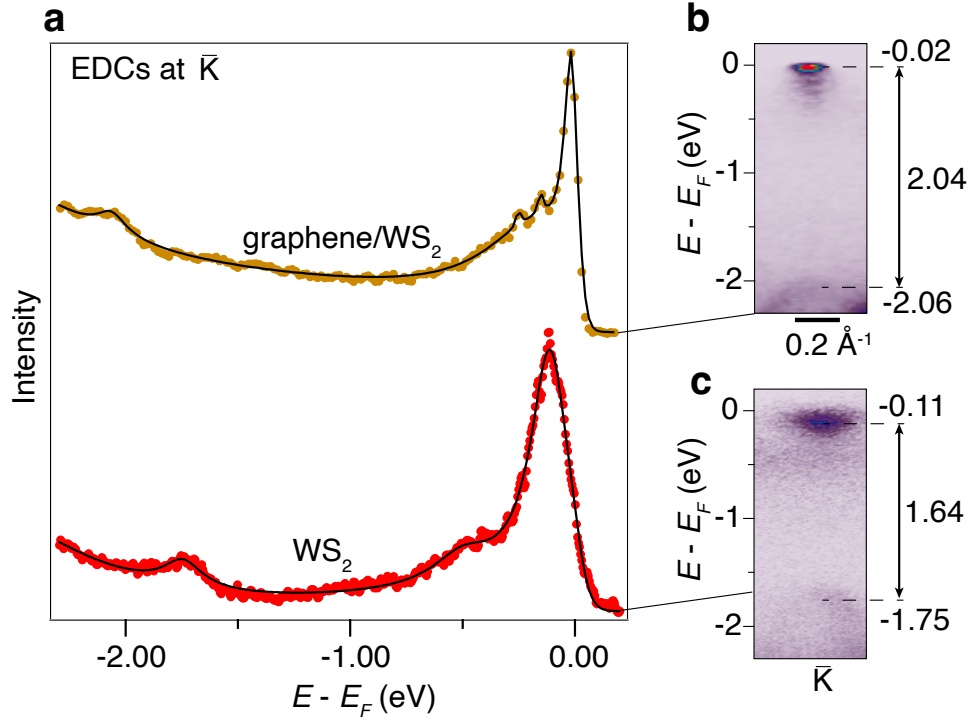


FIG. 5. Extraction of band gaps from ARPES. **a**, Energy distribution curves (EDCs) at \bar{K} in the heavily doped situations shown in Figs. 1(c) and 1(e) of the main paper. The black curves represent fits to a modelled spectral function with several Lorentzian peaks on a linear background and including a Fermi-Dirac cut-off. **b-c**, ARPES spectra around \bar{K} , displaying the VBM and CBM of SL WS₂ (b) with and (c) without a graphene overlayer. VBM and CBM peak positions obtained from the EDC analysis in (a) and the resulting band gaps are stated in units of eV. The error bars are ± 0.02 eV.

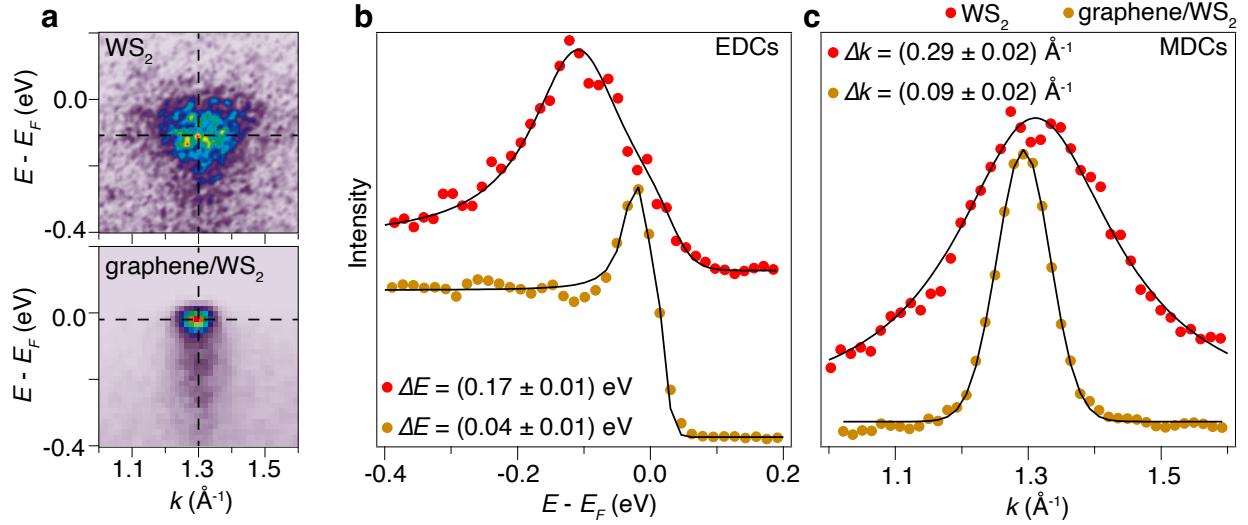


FIG. 6. ARPES linewidths of conduction band states. **a**, ARPES spectra in the conduction band region of WS_2 and $\text{graphene}/\text{WS}_2$, corresponding to the data shown in Figs. 1(d) and 1(f). **b**, EDCs (markers) extracted along the vertical dashed lines in (a) with fits (black curves) to a single Lorentzian peak multiplied by a Fermi-Dirac function. The linewidth of the Lorentzian peak is stated as ΔE . **c**, Momentum distribution curves (MDCs) extracted at the EDC peak energies marked by horizontal dashed lines in (a) and fits to a Lorentzian peak convoluted with a Gaussian. The resulting momentum linewidth is stated as Δk .

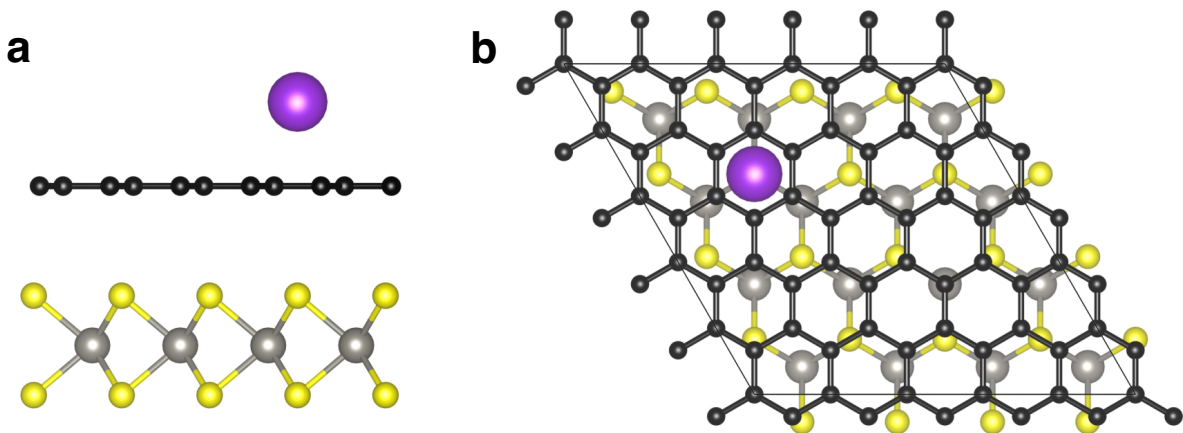


FIG. 7. DFT heterostructure model. **a-b**, View from the (a) side and (b) top of the utilized 4×4 WS_2 / 5×5 graphene supercell with K doping.

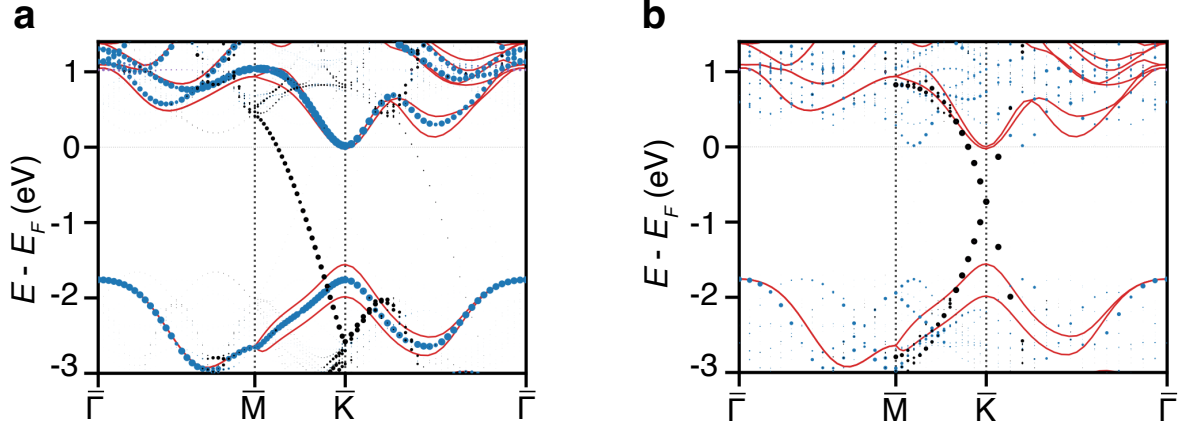


FIG. 8. DFT electronic structure. **a-b**, Band structure of WS_2 with SOC (red line) plotted together with the unfolded band structure without SOC (dots) in the (a) WS_2 and (b) graphene primitive BZs. Blue and black dots represent W and C weights.

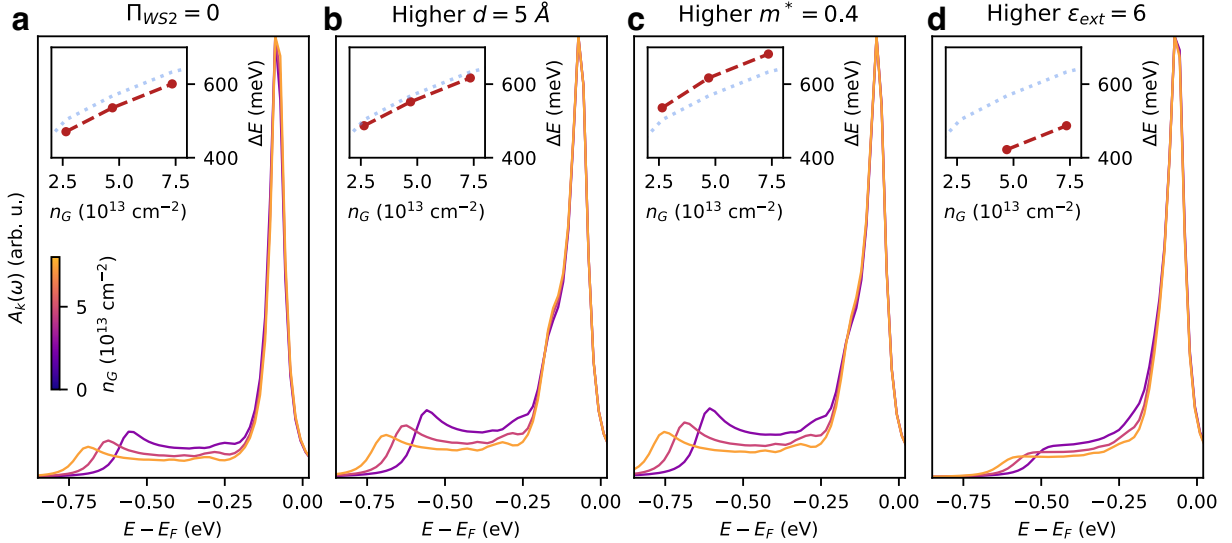


FIG. 9. WS_2 normal state spectral function $A_k(\omega)$ at \bar{K} obtained from G_0W_0 calculations for a variety of graphene occupations. All model parameters are the same as those used in the main text, except for one change per figure. **a**, the WS_2 polarization is set to 0. **b**, the interlayer distance is increased to $d = 5 \text{ \AA}$. **c**, the effective mass is increased to $m^* = 0.4$. **d**, the external dielectric constant is increased to $\epsilon_{ext} = 6$. The insets show the energy splitting ΔE between the WS_2 quasi-particle peak and the plasmon polaron peak as a function of graphene occupation, for the changed model parameters (red dashed) and for the model parameters used in the main text (blue dotted).

* ulstrup@phys.au.dk

† m.roesner@science.ru.nl

‡ jkatoch@andrew.cmu.edu

- [1] D. N. Basov, R. D. Averitt, and D. Hsieh, “Towards properties on demand in quantum materials,” *Nature Materials* **16**, 1077–1088 (2017).
- [2] S. Moser, L. Moreschini, J. Jaćimović, O. S. Barišić, H. Berger, A. Magrez, Y. J. Chang, K. S. Kim, A. Bostwick, E. Rotenberg, L. Forró, and M. Grioni, “Tunable polaronic conduction in anatase TiO₂,” *Phys. Rev. Lett.* **110**, 196403 (2013).
- [3] Z. Wang, S. McKeown Walker, A. Tamai, Y. Wang, Z. Ristic, F. Y. Bruno, A. de la Torre, S. Riccò, N. C. Plumb, M. Shi, P. Hlawenka, J. Sánchez-Barriga, A. Varykhalov, T. K. Kim, M. Hoesch, P. D. C. King, W. Meevasana, U. Diebold, J. Mesot, B. Moritz, T. P. Devereaux, M. Radovic, and F. Baumberger, “Tailoring the nature and strength of electron–phonon interactions in the SrTiO₃(001) 2D electron liquid,” *Nature Materials* **15**, 835–839 (2016).
- [4] Mingu Kang, Sung Won Jung, Woo Jong Shin, Yeongsup Sohn, Sae Hee Ryu, Timur K. Kim, Moritz Hoesch, and Keun Su Kim, “Holstein polaron in a valley-degenerate two-dimensional semiconductor,” *Nature Materials* **17**, 676–680 (2018).
- [5] Chaoyu Chen, José Avila, Shuopei Wang, Yao Wang, Marcin Mucha-Kruczyński, Cheng Shen, Rong Yang, Benjamin Nosarzewski, Thomas P. Devereaux, Guangyu Zhang, and Maria Carmen Asensio, “Emergence of interfacial polarons from electron–phonon coupling in graphene/h-BN van der waals heterostructures,” *Nano Letters* **18**, 1082–1087 (2018).
- [6] Miaomiao Xiang, Xiaochuan Ma, Chang Gao, Ziyang Guo, Chenxi Huang, Yue Xing, Shijing Tan, Jin Zhao, Bing Wang, and Xiang Shao, “Revealing the polaron state at the MoS₂/TiO₂ interface,” *The Journal of Physical Chemistry Letters* **14**, 3360–3367 (2023).
- [7] Fabio Caruso, Henry Lambert, and Feliciano Giustino, “Band structures of plasmonic polarons,” *Phys. Rev. Lett.* **114**, 146404 (2015).
- [8] J. M. Riley, F. Caruso, C. Verdi, L. B. Duffy, M. D. Watson, L. Bawden, K. Volckaert, G. van der Laan, T. Hesjedal, M. Hoesch, F. Giustino, and P. D. C. King, “Crossover from lattice to plasmonic polarons of a spin-polarised electron gas in ferromagnetic EuO,” *Nature Communications* **9**, 2305 (2018).

- [9] Xiaochuan Ma, Zhengwang Cheng, Mingyang Tian, Xiaofeng Liu, Xuefeng Cui, Yaobo Huang, Shijing Tan, Jinlong Yang, and Bing Wang, “Formation of plasmonic polarons in highly electron-doped anatase TiO_2 ,” *Nano Letters* **21**, 430–436 (2021).
- [10] Fabio Caruso, Patrick Amsalem, Jie Ma, Areej Aljarb, Thorsten Schultz, Marios Zacharias, Vincent Tung, Norbert Koch, and Claudia Draxl, “Two-dimensional plasmonic polarons in n -doped monolayer MoS_2 ,” *Phys. Rev. B* **103**, 205152 (2021).
- [11] L. Britnell, R. M. Ribeiro, A. Eckmann, R. Jalil, B. D. Belle, A. Mishchenko, Y.-J. Kim, R. V. Gorbachev, T. Georgiou, S. V. Morozov, A. N. Grigorenko, A. K. Geim, C. Casiraghi, A. H. Castro Neto, and K. S. Novoselov, “Strong light-matter interactions in heterostructures of atomically thin films,” *Science* **340**, 1311–1314 (2013).
- [12] Simon Zihlmann, Aron W. Cummings, Jose H. Garcia, Máté Kedves, Kenji Watanabe, Takashi Taniguchi, Christian Schönenberger, and Péter Makk, “Large spin relaxation anisotropy and valley-zeeman spin-orbit coupling in WSe_2 /graphene/ h -BN heterostructures,” *Phys. Rev. B* **97**, 075434 (2018).
- [13] Harpreet Singh Arora, Robert Polski, Yiran Zhang, Alex Thomson, Youngjoon Choi, Hyunjin Kim, Zhong Lin, Ilham Zaky Wilson, Xiaodong Xu, Jiun-Haw Chu, Kenji Watanabe, Takashi Taniguchi, Jason Alicea, and Stevan Nadj-Perge, “Superconductivity in metallic twisted bilayer graphene stabilized by WSe_2 ,” *Nature* **583**, 379–384 (2020).
- [14] Yanhao Tang, Lizhong Li, Tingxin Li, Yang Xu, Song Liu, Katayun Barmak, Kenji Watanabe, Takashi Taniguchi, Allan H. MacDonald, Jie Shan, and Kin Fai Mak, “Simulation of hubbard model physics in WSe_2/WS_2 moiré superlattices,” *Nature* **579**, 353–358 (2020).
- [15] Emma C. Regan, Danqing Wang, Chenhao Jin, M. Iqbal Bakti Utama, Beini Gao, Xin Wei, Sihan Zhao, Wenyu Zhao, Zuocheng Zhang, Kentaro Yumigeta, Mark Blei, Johan D. Carlström, Kenji Watanabe, Takashi Taniguchi, Sefaattin Tongay, Michael Crommie, Alex Zettl, and Feng Wang, “Mott and generalized wigner crystal states in WSe_2/WS_2 moiré superlattices,” *Nature* **579**, 359–363 (2020).
- [16] Dante M. Kennes, Martin Claassen, Lede Xian, Antoine Georges, Andrew J. Millis, James Hone, Cory R. Dean, D. N. Basov, Abhay N. Pasupathy, and Angel Rubio, “Moiré heterostructures as a condensed-matter quantum simulator,” *Nature Physics* **17**, 155–163 (2021).
- [17] Søren Ulstrup, Cristina E. Giusca, Jill A. Miwa, Charlotte E. Sanders, Alex Browning, Pavel Dudin, Cephise Cacho, Olga Kazakova, D. Kurt Gaskill, Rachael L. Myers-Ward, Tianyi

- Zhang, Mauricio Terrones, and Philip Hofmann, “Nanoscale mapping of quasiparticle band alignment,” *Nature Communications* **10**, 3283 (2019).
- [18] Lutz Waldecker, Archana Raja, Malte Rösner, Christina Steinke, Aaron Bostwick, Roland J. Koch, Chris Jozwiak, Takashi Taniguchi, Kenji Watanabe, Eli Rotenberg, Tim O. Wehling, and Tony F. Heinz, “Rigid band shifts in two-dimensional semiconductors through external dielectric screening,” *Phys. Rev. Lett.* **123**, 206403 (2019).
- [19] Søren Ulstrup, Roland J. Koch, Simranjeet Singh, Kathleen M. McCreary, Berend T. Jonker, Jeremy T. Robinson, Chris Jozwiak, Eli Rotenberg, Aaron Bostwick, Jyoti Katoch, and Jill A. Miwa, “Direct observation of minibands in a twisted graphene/WS₂ bilayer,” *Science Advances* **6**, eaay6104 (2020).
- [20] Saien Xie, Brendan D. Faeth, Yanhao Tang, Lizhong Li, Eli Gerber, Christopher T. Parzyck, Debanjan Chowdhury, Ya-Hui Zhang, Christopher Jozwiak, Aaron Bostwick, Eli Rotenberg, Eun-Ah Kim, Jie Shan, Kin Fai Mak, and Kyle M. Shen, “Strong interlayer interactions in bilayer and trilayer moiré superlattices,” *Science Advances* **8**, eabk1911 (2022).
- [21] Zachariah Hennighausen, Jisoo Moon, Kathleen M. McCreary, Connie H. Li, Olaf M. J. van ’t Erve, and Berend T. Jonker, “Interlayer exciton–phonon bound state in Bi₂Se₃/monolayer WS₂ van der waals heterostructures,” *ACS Nano* **17**, 2529–2536 (2023).
- [22] Paul V. Nguyen, Natalie C. Teutsch, Nathan P. Wilson, Joshua Kahn, Xue Xia, Abigail J. Graham, Viktor Kandyba, Alessio Giampietri, Alexei Barinov, Gabriel C. Constantinescu, Nelson Yeung, Nicholas D. M. Hine, Xiaodong Xu, David H. Cobden, and Neil R. Wilson, “Visualizing electrostatic gating effects in two-dimensional heterostructures,” *Nature* **572**, 220–223 (2019).
- [23] Hsun-Jen Chuang, Xuebin Tan, Nirmal Jeevi Ghimire, Meeghage Madusanka Perera, Bhim Chamlagain, Mark Ming-Cheng Cheng, Jiaqiang Yan, David Mandrus, David Tománek, and Zhixian Zhou, “High mobility WSe₂ p- and n-type field-effect transistors contacted by highly doped graphene for low-resistance contacts,” *Nano Letters* **14**, 3594–3601 (2014).
- [24] Xu Cui, Gwan-Hyoung Lee, Young Duck Kim, Ghidewon Arefe, Pinshane Y. Huang, Chul-Ho Lee, Daniel A. Chenet, Xian Zhang, Lei Wang, Fan Ye, Filippo Pizzocchero, Bjarke S. Jessen, Kenji Watanabe, Takashi Taniguchi, David A. Muller, Tony Low, Philip Kim, and James Hone, “Multi-terminal transport measurements of MoS₂ using a van der waals heterostructure device platform,” *Nature Nanotechnology* **10**, 534–540 (2015).

- [25] Yuan Liu, Hao Wu, Hung-Chieh Cheng, Sen Yang, Enbo Zhu, Qiyuan He, Mengning Ding, Dehui Li, Jian Guo, Nathan O. Weiss, Yu Huang, and Xiangfeng Duan, “Toward barrier free contact to molybdenum disulfide using graphene electrodes,” *Nano Letters* **15**, 3030–3034 (2015).
- [26] Riccardo Pisoni, Yongjin Lee, Hiske Overweg, Marius Eich, Pauline Simonet, Kenji Watanabe, Takashi Taniguchi, Roman Gorbachev, Thomas Ihn, and Klaus Ensslin, “Gate-defined one-dimensional channel and broken symmetry states in MoS₂ van der waals heterostructures,” *Nano Letters* **17**, 5008–5011 (2017).
- [27] Sang-Soo Chee, Dongpyo Seo, Hanggyu Kim, Hanbyeol Jang, Seungmin Lee, Seung Pil Moon, Kyu Hyoung Lee, Sung Wng Kim, Hyunyong Choi, and Moon-Ho Ham, “Lowering the schottky barrier height by graphene/Ag electrodes for high-mobility MoS₂ field-effect transistors,” *Advanced Materials* **31**, 1804422 (2019).
- [28] Jyoti Katoch, Søren Ulstrup, Roland J. Koch, Simon Moser, Kathleen M. McCreary, Simranjeet Singh, Jinsong Xu, Berend T. Jonker, Roland K. Kawakami, Aaron Bostwick, Eli Rotenberg, and Chris Jozwiak, “Giant spin-splitting and gap renormalization driven by trions in single-layer WS₂/h-BN heterostructures,” *Nature Physics* **14**, 355–359 (2018).
- [29] Nicki Frank Hinsche, Arlette S. Ngankeu, Kevin Guilloy, Sanjoy K. Mahatha, Antonija Grubišić Čabo, Marco Bianchi, Maciej Dendzik, Charlotte E. Sanders, Jill A. Miwa, Harsh Bana, Elisabetta Travaglia, Paolo Lacovig, Luca Bignardi, Rosanna Larciprete, Alessandro Baraldi, Silvano Lizzit, Kristian Sommer Thygesen, and Philip Hofmann, “Spin-dependent electron-phonon coupling in the valence band of single-layer WS₂,” *Phys. Rev. B* **96**, 121402 (2017).
- [30] Z. Y. Zhu, Y. C. Cheng, and U. Schwingenschlögl, “Giant spin-orbit-induced spin splitting in two-dimensional transition-metal dichalcogenide semiconductors,” *Phys. Rev. B* **84**, 153402 (2011).
- [31] Weng Hong Sio and Feliciano Giustino, “Polarons in two-dimensional atomic crystals,” *Nature Physics* **19**, 629–636 (2023).
- [32] Ayse Berkdemir, Humberto R. Gutiérrez, Andrés R. Botello-Méndez, Néstor Perea-López, Ana Laura Elías, Chen-Ing Chia, Bei Wang, Vincent H. Crespi, Florentino López-Urías, Jean-Christophe Charlier, Humberto Terrones, and Mauricio Terrones, “Identification of individual and few layers of WS₂ using raman spectroscopy,” *Scientific Reports* **3**, 1755 (2013).

- [33] Dino Novko, “Dopant-induced plasmon decay in graphene,” *Nano Letters* **17**, 6991–6996 (2017).
- [34] E. R. Margine, Henry Lambert, and Feliciano Giustino, “Electron-phonon interaction and pairing mechanism in superconducting Ca-intercalated bilayer graphene,” *Scientific Reports* **6**, 21414 (2016).
- [35] Aaron Bostwick, Florian Speck, Thomas Seyller, Karsten Horn, Marco Polini, Reza Asgari, Allan H. MacDonald, and Eli Rotenberg, “Observation of plasmarons in quasi-freestanding doped graphene,” *Science* **328**, 999–1002 (2010).
- [36] Frank H. L. Koppens, Darrick E. Chang, and F. Javier García de Abajo, “Graphene plasmonics: A platform for strong light–matter interactions,” *Nano Letters* **11**, 3370–3377 (2011).
- [37] A. N. Grigorenko, M. Polini, and K. S. Novoselov, “Graphene plasmonics,” *Nature Photonics* **6**, 749–758 (2012).
- [38] F. Aryasetiawan, L. Hedin, and K. Karlsson, “Multiple plasmon satellites in Na and Al spectral functions from ab initio cumulant expansion,” *Physical Review Letters* **77**, 2268–2271 (1996).
- [39] Matteo Guzzo, Giovanna Lani, Francesco Sottile, Pina Romaniello, Matteo Gatti, Joshua J. Kas, John J. Rehr, Mathieu G. Silly, Fausto Sirotti, and Lucia Reining, “Valence electron photoemission spectrum of semiconductors: Ab initio description of multiple satellites,” *Physical Review Letters* **107**, 166401 (2011).
- [40] Fabio Caruso and Feliciano Giustino, “The GW plus cumulant method and plasmonic polarons: application to the homogeneous electron gas*,” *The European Physical Journal B* **89**, 238 (2016).
- [41] P. Zhang, P. Richard, T. Qian, Y.-M. Xu, X. Dai, and H. Ding, “A precise method for visualizing dispersive features in image plots,” *Review of Scientific Instruments* **82**, 043712 (2011).
- [42] Daniel Hernangómez-Pérez, Andrea Donarini, and Sivan Refaely-Abramson, “Charge quenching at defect states in transition metal dichalcogenide–graphene van der waals heterobilayers,” *Physical Review B* **107**, 075419 (2023).
- [43] G. Kresse and J. Hafner, “Ab initio molecular dynamics for liquid metals,” *Physical Review B* **47**, 558–561 (1993).
- [44] G. Kresse and J. Furthmüller, “Efficient iterative schemes for ab initio total-energy calculations

- using a plane-wave basis set,” *Physical Review B* **54**, 11169–11186 (1996).
- [45] G. Kresse and D. Joubert, “From ultrasoft pseudopotentials to the projector augmented-wave method,” *Physical Review B* **59**, 1758–1775 (1999).
- [46] P. E. Blöchl, “Projector augmented-wave method,” *Physical Review B* **50**, 17953–17979 (1994).
- [47] John P. Perdew, Kieron Burke, and Matthias Ernzerhof, “Generalized gradient approximation made simple,” *Physical Review Letters* **77**, 3865–3868 (1996).
- [48] Voicu Popescu and Alex Zunger, “Extracting e vs k effective band structure from supercell calculations on alloys and impurities,” *Physical Review B* **85**, 085201 (2012).
- [49] Qijing Zheng, “QijingZheng/VaspBandUnfolding,” (2023), original-date: 2017-05-08T08:51:01Z.
- [50] Niklas Hofmann, Leonard Weigl, Johannes Gradl, Neeraj Mishra, Giorgio Orlandini, Stiven Forti, Camilla Coletti, Simone Latini, Lede Xian, Angel Rubio, Dilan Perez Paredes, Raul Perea Causin, Samuel Brem, Ermin Malic, and Isabella Gierz, “Link between interlayer hybridization and ultrafast charge transfer in WS_2 -graphene heterostructures,” *2D Materials* **10**, 035025 (2023).
- [51] M. Rösner, E. Şaşıoğlu, C. Friedrich, S. Blügel, and T. O. Wehling, “Wannier function approach to realistic Coulomb interactions in layered materials and heterostructures,” *Physical Review B* **92**, 085102 (2015), publisher: American Physical Society.
- [52] C. Steinke, T. O. Wehling, and M. Rösner, “Coulomb-engineered heterojunctions and dynamical screening in transition metal dichalcogenide monolayers,” *Physical Review B* **102**, 115111 (2020).
- [53] Olivier Parcollet, Michel Ferrero, Thomas Ayrál, Hartmut Hafermann, Igor Krivenko, Laura Messio, and Priyanka Seth, “TRIQS: A toolbox for research on interacting quantum systems,” *Computer Physics Communications* **196**, 398–415 (2015).
- [54] Nils Wentzell, Hugo U.R. Strand, Stefan Kaeser, Dylan Simon, Alexander Hampel, Egcvanloon, Olivier Parcollet, D. Philipp, and Manuel Zingl, “TRIQS/tprf: Version 3.1.1,” (2022).
- [55] Gabriele Giuliani and Giovanni Vignale, Quantum Theory of the Electron Liquid (Cambridge University Press, Cambridge, 2005).
- [56] B Wunsch, T Stauber, F Sols, and F Guinea, “Dynamical polarization of graphene at finite

- doping,” *New Journal of Physics* **8**, 318–318 (2006).
- [57] E. H. Hwang and S. Das Sarma, “Dielectric function, screening, and plasmons in two-dimensional graphene,” *Physical Review B* **75**, 205418 (2007).
- [58] L. V. Keldysh, “Coulomb interaction in thin semiconductor and semimetal films,” *Soviet Journal of Experimental and Theoretical Physics Letters* **29**, 658 (1979).